Materials Today Bio 6 (2020) 100045

Contents lists available at ScienceDirect

Materials Today Bio

journal homepage: www.journals.elsevier.com/materials-today-bio

Functionalized DNA-spider silk nanohydrogels for controlled protein binding and release

Martin Humenik [a,*], Tamara Preiß [a], Sebastian Gödrich [b], Georg Papastavrou [b,c,f], Thomas Scheibel [a,c,d,e,f]

[a] Department of Biomaterials, Faculty of Engineering Science, Universität Bayreuth, Prof.-Rüdiger-Bormann.Str. 1, 95447 Bayreuth, Germany
[b] Department of Physical Chemistry II, Faculty of Biology, Chemistry & Earth Sciences, Universität Bayreuth, Universitätsstraße 30, 95440 Bayreuth, Germany
[c] Bayreuth Center for Colloids and Interfaces (BZKG), Universität Bayreuth, Universitätsstraße 30, 95440 Bayreuth, Germany
[d] Bayreuth Center for Molecular Biosciences (BZMB), Universität Bayreuth, Universitätsstraße 30, 95440 Bayreuth, Germany
[e] Bayreuth Center for Material Science (BayMAT), Universität Bayreuth, Universitätsstraße 30, 95440 Bayreuth, Germany
[f] Bavarian Polymer Institute (BPI), Universität Bayreuth, Universitätsstraße 30, 95440 Bayreuth, Germany

ARTICLE INFO

Keywords:
aptamers
nanohydrogels
recombinant spider silk
self-assembly
thrombin

ABSTRACT

Hydrogels are excellent scaffolds to accommodate sensitive enzymes in a protective environment. However, the lack of suitable immobilization techniques on substrates and the lack of selectivity to anchor a biocatalyst are major drawbacks preventing the use of hydrogels in bioanalytical devices. Here, nanofilm coatings on surfaces were made of a recombinant spider silk protein (rssp) to induce rssp self-assembly and thus the formation of fibril-based nanohydrogels. To functionalize spider silk nanohydrogels for bioselective binding of proteins, two different antithrombin aptamers were chemically conjugated with the rssp, thereby integrating the target-binding function into the nanohydrogel network. Human thrombin was selected as a sensitive model target, in which the structural integrity determines its activity. The chosen aptamers, which bind various exosites of thrombin, enabled selective and cooperative embedding of the protein into the nanohydrogels. The change of the aptamer secondary structure using complementary DNA sequences led to the release of active thrombin and confirmed the addressable functionalization of spider silk nanohydrogels.

1. Introduction

In a pioneering work by Updike and Hicks, a first biosensor used glucose oxidase immobilized in a gel to produce an amperometric readout reporting the concentration of glucose [1]. Nowadays developments focus on point-of-care diagnostics of biomarkers and pathogen detection in food and dairy industry. Antibodies are used routinely in biomedical diagnostics in enzyme-linked immunosorbent assays reporting via the specific formation of immune complexes [2] or immuno-polymerase chain reaction [3] of clinically relevant markers [4]. Catalytic enzymes are very attractive for biosensor applications because of a variety of measurable reaction products frequently monitored via optical or electrochemical readouts [5]. Enzymes are typically anchored at surface structures, allowing short diffusion pathways between the biorecognition element and the transducer [6–9]. Although antibody and enzyme-based biosensors are most frequently used in the praxis, they are prone to structural changes (denaturation), loss of activity, and degradation due to environmental changes in pH, moisture, and/or temperature, making reproducibility of biosensors challenging and industrial processing costly. Thus, aptamers [10] and nature-inspired molecularly imprinted hydrogels [11] are proposed as an alternative to protein-based biosensors. Aptamers are single-stranded oligonucleotides acquired in a selection process called systemic evolution of ligands by exponential enrichment (SELEX). This procedure generates a library of 10^{13}–10^{15} randomly generated sequences and applies screening, target binding, and selection steps to generate and amplify aptamer ligands with high binding affinities (nM to pM levels, similar to antibodies). Moreover, chemical synthesis of aptamers is well-defined and highly reproducible, enabling the production of robust biorecognition elements [12]. The range of analytes is virtually unlimited as demonstrated by the plethora of aptamer targets such as metal ions, organic molecules, peptides, proteins, or whole cells [13–15].

Abovementioned conventional biorecognition elements often face low activity issues because of non-specific adsorption, structural

* Corresponding author.
E-mail address: martin.humenik@bm.uni-bayreuth.de (M. Humenik).

https://doi.org/10.1016/j.mtbio.2020.100045
Received 20 December 2019; Received in revised form 6 February 2020; Accepted 7 February 2020
Available online 24 February 2020

disintegration as well as restricted accessibility of biocatalysts on two-dimensional (2D) substrates [16]. However, 3D-networks, as represented by hydrogels, have been successfully utilized to accommodate bioactive antibodies, enzymes, or nucleic acids [17–19] in different applications [20–22]. Hydrogels are interconnected by chemical or physical crosslinks, which provide integrity concerning their mechanical and physical properties [20,23–25]. High surface area and water content of hydrogels enable native-like environments with low spatial restrictions of entrapped biocatalysts [21,22,26]. Nonetheless, hydrogels possess typically low adhesiveness toward biomacromolecules because of osmotic pressure of the swollen network. Further, the lack of biocompatible immobilization of a hydrogel on solid supports represents a major drawback concerning the development of devices [27,28]. Attempts to specifically coat a substrate surface used setups with silk-elastin–like proteins [29], collagen-mimetic peptides [30], peptide-amphiphiles [31], and spider silk–like proteins [32]. However, many surface parameters influenced their self-assembly such as electrostatic interactions, hydrophilic/hydrophobic interactions, surface topography and roughness, and surface confinement [33–38].

Previously, we have shown that spider silk surfaces can trigger nanofibril assembly in suspensions [39]. Further, DNA-directed immobilization of recombinant spider silk proteins (rssp) allowed nanofibril growth on 2D surfaces [40] as well. In the present work, we utilized controllable molecular self-assembly of spider silk fibrils on rssp nanofilms (nf), which were applied to create 'seeding surfaces' to self-assemble rssp nanohydrogels (nh) on an arbitrary substrate (su). Upon the nanohydrogel functionalization with aptamers, protein targets of interest could be selectively bound as well as released on demand (Scheme 1). Human thrombin was used herein as a model target in which the enzymatic activity is closely related to its native structure. This allows assessment of the nanohydrogel biocompatibility in relation to accommodation of environmentally sensitive targets. At the same time, we chose functionalization of the nanohydrogels using DNA-based aptamers enabling reversible binding as well as inhibition of the model enzyme into the nanofibrillar hydrogel network via biorecognition.

2. Materials and methods

2.1. Materials

All chemicals were purchased from Roth (Karlsruhe, Germany) in analytical grade, if not stated otherwise. Recombinant spider silk protein eADF4(C16) was purchased from AMSilk GmbH (Planegg/München,Germany). Ultrapure water in the experiments was obtained using a Merck Millipore system (Billerica, MA).

2.2. Preparation of apt-rssp conjugates

The descriptions for preparation of starting azide-modified rssps (N3-rssp) and 5′-dibenzocyclooctyne (DBCO)-modified aptamers are included in Supporting information.

The azido-modified rssp was mixed with two eq. of DBCO-

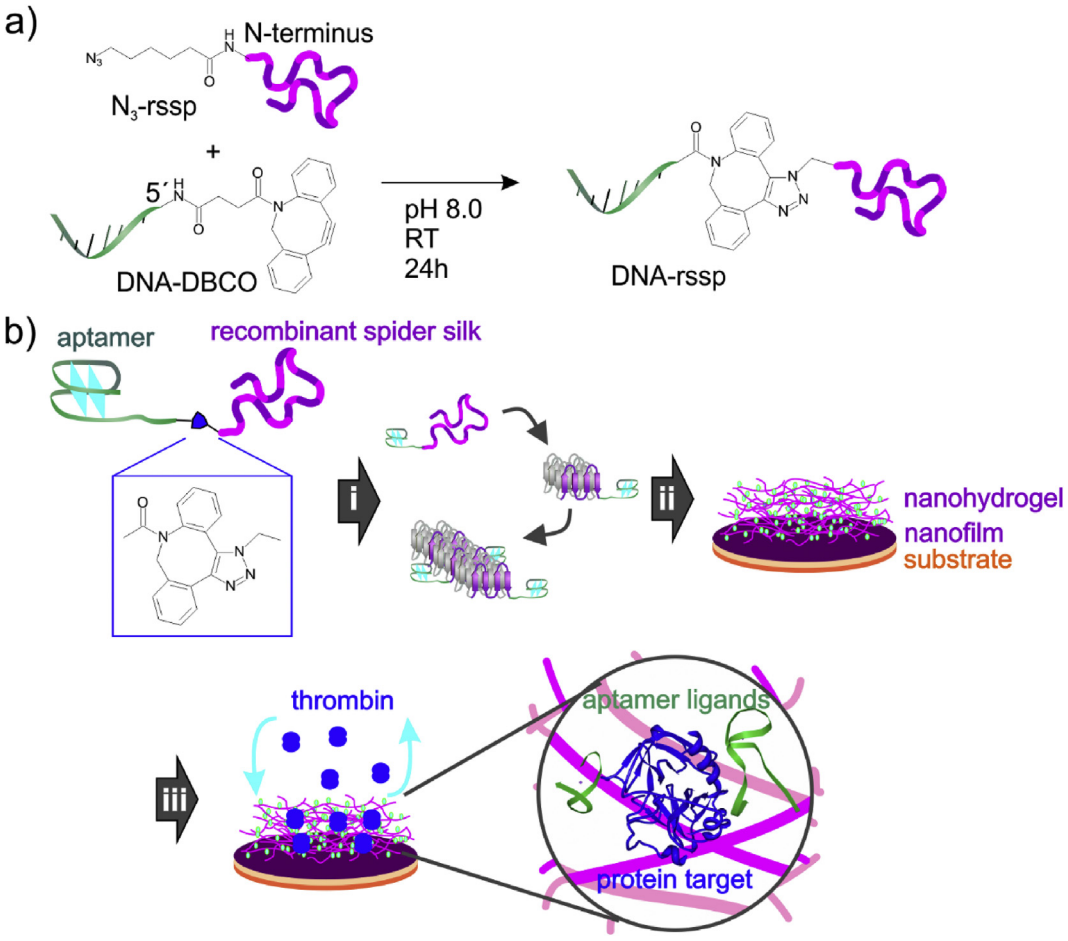

Scheme 1. Nanohydrogel assembly. (a) Coupling of azide-modified recombinant spider silk protein (N_3-rssp) with 5′-dibenzocyclooctyne-modified DNA (DNA-DBCO) yields hybrid building blocks; (b) The recombinant spider silk protein (rssp) self-assembles and DNA sequences fold into aptamers (apt) yielding aptamer-functionalized nanofibrils (i). A substrate coated with rssp nanofilm generated a 'seeding surface' enabling rssp fibrilization thereon. High density of fibrils and formation of physical crosslinks resulted in a confined nanohydrogel. Utilization of aptamer ligands in rssp nanohydrogels (green dots) (ii) allows deposition as well as triggered release of specific targets (e.g. thrombin) (iii). Structures of thrombin and aptamers in the magnified view are adopted from pdb 5EW1 [41].

oligonucleotide in 50 mM HEPES buffer, pH 8 and 4 M urea (Fig. S1a). The cycloaddition reaction was incubated at RT, and the depletion of the protein was monitored using a size-exclusion chromatography (SEC) column (Yarra™ SEC-4000) in 25 mM Tris/HCl, pH 7.0, 100 mM NaCl (Fig. S1c and d) for 48 h. Apt-rssp conjugates were purified by precipitation using an equivalent of 2 M potassium phosphate buffer, pH 8 [42], and the excess of oligonucleotides was removed using a washing buffer (100 mM Tris/HCl, pH 7.0, 300 mM NaCl). This simplified procedure omitted column-based purifications [43], thus enabling the scale-up of the process. The conjugates were obtained in yields of 60–65% in respect to the starting N_3-rssp, and their identity was confirmed using an Agilent 1100 HPLC system (Agilent, Waldbronn, Germany) on a SEC column (Superose 6 10/300 GL; GE Healthcare Europe GmbH, Freiburg im Breisgau, Germany) in ion-depleted Tris base (89 mM), Boric acid (89 mM), EDTA (2 mM), pH 8.0 (TBE)-buffers and Na^+/K^+ rich Gq-buffers coupled to a multiangle light scattering (MALS) detector DOWN-EOS (Wyatt, Dernbach, Germany) (Fig. S1d) as described previously [43].

2.3. CD spectroscopy

Far-UV spectra of conjugates (Fig. 1a) were recorded at 0.15 mg/mL protein in aqueous buffers (TBE-buffer: 89 mM Tris, 89 mM boric acid, 20 mM EDTA, pH 8.0; Gq-buffer: 25 mM HEPES, pH 8.0, 200 mM NaCl, 20 mM KCl, K-Pi: 10 mM Tris/HCl, 150 mM $K_xH_yPO_4$ pH 8.0) using a J-815 CD spectrometer (Jasco, Pfungstadt, Germany). Scans were accumulated 5 times at a scan speed of 100 nm/min, response time of 0.5 s, acquisition interval of 0.1 nm, and bandwidth of 1 nm at 22 °C.

2.4. Binding of the conjugates to thrombin

The apt-rssp conjugates (1 μM) were mixed with equimolar amounts of human α-thrombin (Thermo Fisher Scientific Inc., Waltham, MA) in Gq-buffer (25 mM HEPES-Na, pH 8.0, 200 mM NaCl, 20 mM KCl) at RT for 30 min. The equivalent of 0.1 nm thrombin was loaded on the SEC column (Yarra™ SEC-4000, 3 μm, LC Column, 300 × 4.6 mm;

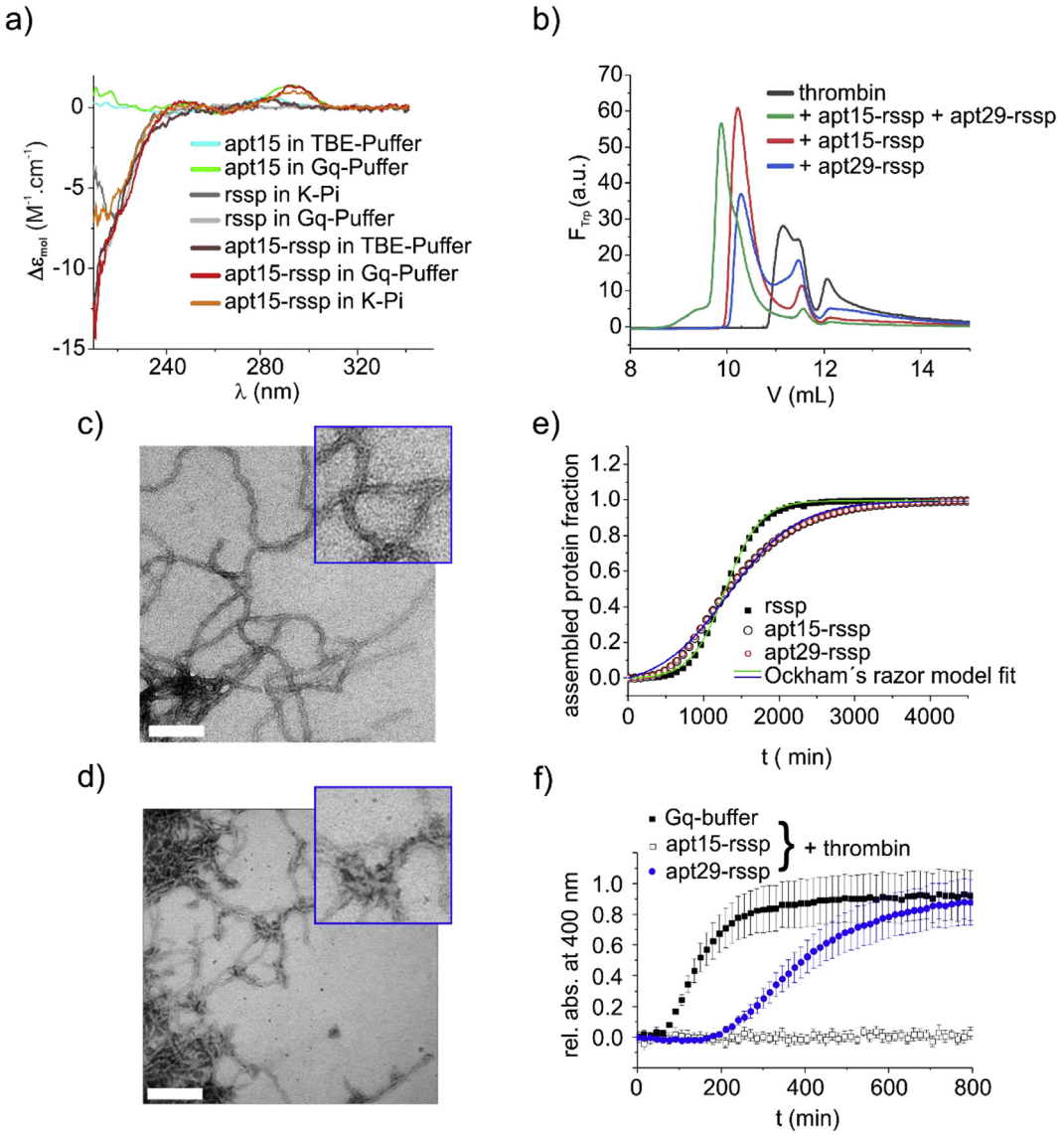

Fig. 1. Functional analysis of apt-rssp conjugates. (a) Far UV-CD spectra of the aptamer oligonucleotide, rssp and the corresponding conjugate in ion-depleted TBE-buffer (89 mM Tris, 89 mM boric acid, 20 mM EDTA, pH 8.0) as well as Na^+/K^+ rich Gq-buffer (25 mM HEPES, pH 8.0, 200 mM NaCl, 20 mM KCl); (b) SEC analysis of thrombin binding to the conjugates (Yarra SEC-4000 column in Gq-buffer and detection of thrombin-specific tryptophan fluorescence); (c) and (d) TEM of rssp and apt15-rssp fibrils after treatment with thrombin; (e) Fibril self-assembly kinetics of unmodified rssp and corresponding conjugates monitored using turbidity at 340 nm as published previously [45]; (f) Coagulation of fibrin upon fibrinogen-cleavage catalyzed by thrombin without or in the presence of apt-conjugates as indicated. Scale bars 100 nm in (c) and (d) and 50 nm for the inserts. SEC, size-exclusion chromatography; TEM, transmission electron microscopy; rssp, recombinant spider silk protein.

Phenomenex Ltd., Aschaffenburg, Germany) using the Gq-buffer as a mobile phase and a Jasco-HPLC system equipped with a fluorescence detector. The shift in the mobility of thrombin in dependence of the apt-rssp presence (Fig. 1b) was monitored using thrombin-specific tryptophan fluorescence with an excitation wavelength of 295 nm and emission wavelength of 350 nm.

2.5. Transmission electron microscopy

Samples for transmission electron microscopy (TEM) were prepared as described previously [43]. Briefly, 2 μL of the fibril suspensions were spotted on supports (Pioloform-carbon-coated 200-mesh copper grids [Plano GmbH, Wetzlar, Germany]), incubated for 2 min, washed with 5 μL of ddH2O four times. In addition, the dry fibrils were treated on the TEM grids using 5 nM thrombin and 10 μM human serum albumin (HSA) (Sigma-Aldrich Chemie GmbH, Schnelldorf, Germany) in Gq-buffer (Fig. 1c and d) for 30 min before applying the washing buffer (2 × 5 μl; 100 mM Tris/HCl, pH 7.0, 300 mM NaCl) and H_2O (2 × 5 μl). Finally, uranyl acetate (2% w/v) was used as a contrasting agent for 1 min, and blotted samples were dried at ambient conditions for 16 h before imaging.

2.6. Rssp self-assembly in solution

Self-assembly of the unmodified rssp was compared to that of apt-rssp conjugates at 15 μM rssp/conjugate in 150 mM K-Pi, pH 8 at 20 °C using turbidity monitoring at 340 nm (Fig. 1e) in a Varian Cary® 50 UV–Vis Spectrophotometer (Agilent) as described previously [44]. The conjugates showed assembly kinetics with similar sigmoidal shapes [45], however, slightly slower growth phases ($k_{growth} = 1.37$ and 1.35×10^{-4} vs. 2.90×10^{-4} μM min^{-1} for apt15-and apt29-rssp vs. rssp) in comparison to that of the unmodified rssp.

2.7. Coagulation assay

The inhibitory activity of the apt-rssp was tested adopting the coagulation assay from Refs. [46,47]. Thrombin (5.9 nM) was treated with apt-rssp (400 nM) in the presence of human fibrinogen (Thermo Fisher) (2 μM) and HSA (10 μM) in clotting buffer (25 mM Tris/HCl, pH 7.4, 150 mM NaCl, 5 mM KCl, 1 mM $MgCl_2$, 1 mM $CaCl_2$). The formation of fibrin was monitored using turbidity evolution at 400 nm.

2.8. Atomic force microscopy

Atomic force microscopy (AFM) imaging of dry nanofilm samples was performed on a Dimension™ ICON with Nanoscope V controller (Bruker, Santa Barbara, CA) in TappingMode™ using Si cantilevers (OTESPA-R3, f_0 300 kHz, k: 26 N/m, Bruker) as described previously [43]. To analyze the swelling behavior of the nanohydrogels, AFM measurements were performed in air as well as aqueous solutions using PeakForce Tapping™ mode and standard cantilevers for liquid imaging (Bruker SNL) with a nominal spring constant of 0.35 N/m. A PeakForce Tapping™ frequency of 2 kHz and amplitude of ~100 nm was used. Before each measurement, the optical lever sensitivity and the spring constant were calibrated using the software of the AFM (Nanoscope 9.10). For the swelling/deswelling cycles, a PeakForce setpoint of 1 nN was applied, whereas for deformation measurements, 5 nN was used. After each measurement in water, the liquid was removed, and the protein nanohydrogel was dried *in situ* at 40 °C using a Bruker heater chuck connected to a LakeShore 335 temperature controller (Lake Shore Cryotronics). Data processing was performed using Nanoscope Analysis 1.40 (Bruker).

2.9. Preparation of rssp nanofilms

Silicon wafers (~1 cm^2) were cleaned using a mixture of $H_2O/NH_3/H_2O_2$ as described previously [40], and rssp (1% solution in formic acid, 20 μL) was placed in the center of the substrate and spin-coated using a 1-EC 101 DT-19456 Spin-Coater (Headway Research Inc., Garland, TX) at 4000 rpm. The film was treated using MeOH vapor applying 20 mL methanol at the bottom of a desiccator, which was evacuated (p~10 mbar) to generate a saturated methanol atmosphere. Samples were incubated for 24 h to induce the protein transformation into a water-insoluble beta-sheet rich state as described previously [48,49].

2.10. Preparation of nanohydrogels

Nanofilms on Si-wafers were placed into 24 well plates, and hydrogel self-assembly was initiated using 10 μM rssp or the respective conjugate in 100 mM KPi for 24 h. The nf/nh substrate was washed using the washing buffer, Gq-buffer, and MQ H_2O (300 μL each). The nanohydrogels were dried using filtered nitrogen stream (0.2 μm filter) and stored at 4 °C before further use.

2.11. Thrombin activity assay

Non-treated 96 well pates (μClear®, Greiner Bio-One GmbH, Frickenhausen, Germany) (0.32 cm^2) were incubated with rssp solution (0.5 mg protein/cm^2, 0.5% w/v protein in hexafluoroisopropanol [abcr GmbH, Karlsruhe, Germany]) for 16 h in a fume hood. Rssp films were treated using 80 μL of MeOH per well in open plates for 16 h to induce β-sheet formation [48]. The dried films in the wells were washed using the washing buffer and MQ H_2O (300 μL each), and nanohydrogels were prepared on top as described above. Thrombin (7 nM) was added in clotting buffer containing 10 μM HSA and incubated at RT applying gentle shaking for 30 min. The activity of the unbound thrombin was determined upon addition of the internally quenched 5-FAM/QXL™ 520 FRET peptide (from SensoLyte® 520 Thrombin Activity Assay Kit; Eurogentec S.A., Belgium) (5 μM, thrombin substrate). The evolution of the fluorescein fluorescence signal after substrate-cleavage was monitored using a microplate reader (Mithras LB 940; Berthold Technologies GmbH & Co. KG, Bad Wildbad, Germany) over 9 h. In the case of thrombin release from the aptamer-modified nanohydrogels, 1 μM complementary oligonucleotides (Table S1) were added to the assay after 9 h and the monitoring continued for another 5 h.

2.12. Statistical analysis

The experimental data were analyzed (n = 3–5) as indicated in the description of the methods and figures and evaluated statistically using arithmetic mean and standard deviation (SD), represented by error bars in the graphs (+/− values from the arithmetic mean). In case of thrombin activity on different surfaces (Fig. 2F), significance of data variance was tested using Origin 8.0. First, the normal distribution of the collected data was tested using Shapiro-Wilk statistics. T-test was used to evaluate differences between the pairs of analyzed samples, whereas the differences were assumed significant at $p < 0.05$.

3. Results and discussions

3.1. Synthesis of building blocks and functional tests

The rssp eADF4(C16) self-assembles into cross-β fibrils without interfering with the functionality of chemically conjugated nucleic acids or even genetically fused globular proteins [43,44,50]. Here, rssp was functionalized with DNA aptamers (apt). DNA aptamers have been shown to be stable, easily accessible by commercial synthesis, and thus represent a suitable material for the development of biosensors or drug delivery carriers [51,52]. We used 15 and 29 base sequences (Table S1), which have been predicted to bind thrombin with a low K_D in the nM range. Apt15 is selective for thrombin exosite I and inhibits its proteolytic activity, whereas apt29 binds to exosite II, a heparin binding regulatory site [41,53–56].

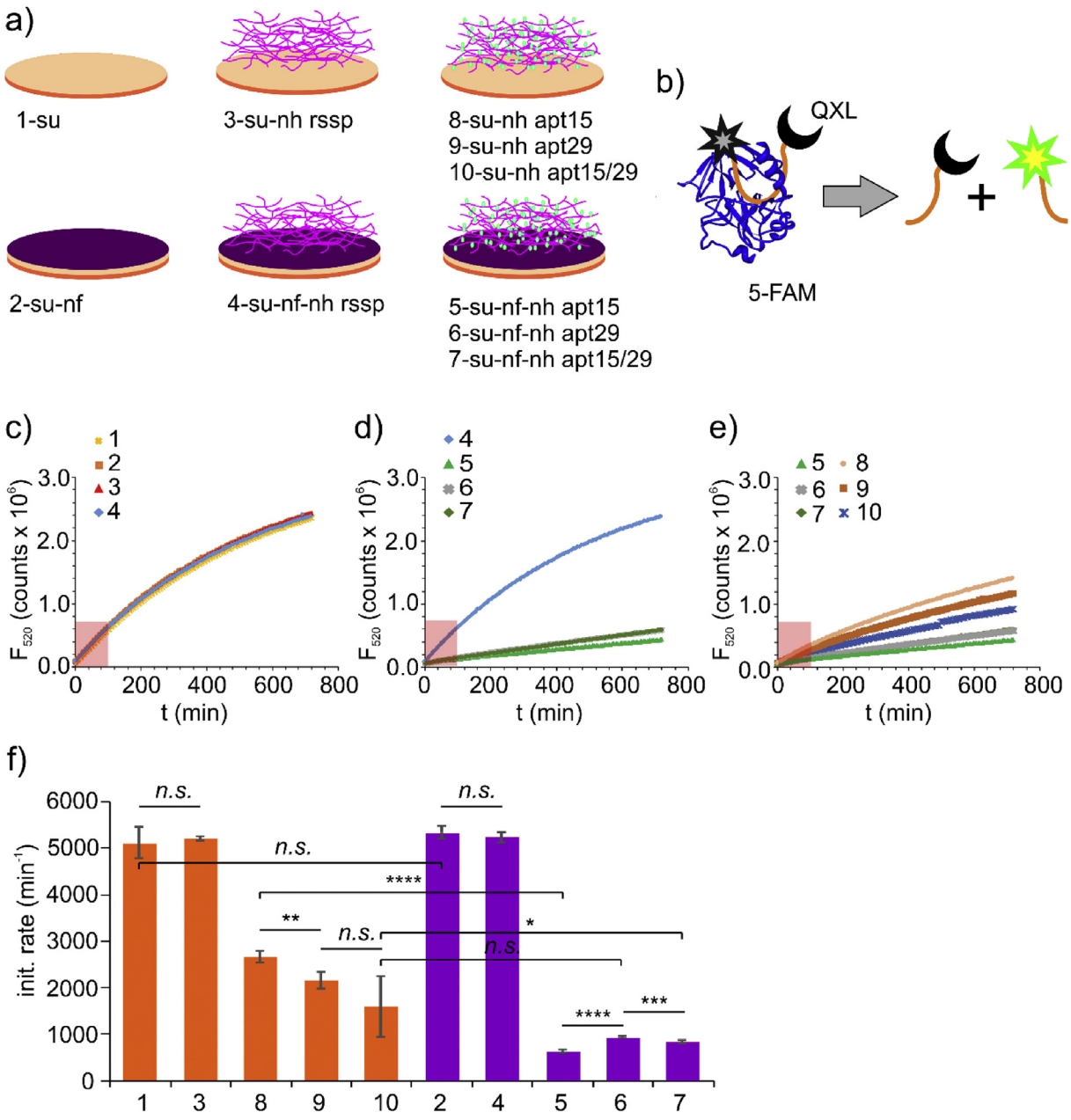

Fig. 2. Binding and activity of thrombin on DNA-spider silk nanohydrogels. (a) Surface setups: (1) polystyrene substrate (su), (2) su + rssp nanofilm, (3) su + rssp nanohydrogel (nh); (4) su + nf + rssp nh, (5–7) su + nf + nh made of apt15 (5) apt29 (6) and 1:1 mix of 15/29-rssp conjugates (7), (8–10) su with the same nanohydrogels as in 5–7 but without the rssp nanofilm layer underneath; (b) Scheme showing the cleavage of a peptide substrate upon hydrolytic activity of thrombin, resulting in the release of a fluorescent probe from the quencher yielding a fluorescence signal; (c)–(e) After incubation of thrombin with the depicted surfaces (1–10), its enzymatic activity was assayed using a FRET substrate (n = 5). The boxed area represents the initial 100 min of the thrombin FRET assay used to calculate the slopes presented in (f); (samples per condition n = 5; error bars = +/− SD, significance of differences in f) estimated by *t*-tests; *n.s.* not significant, $*p < 0.05$; $**p < 0.01$; $***p < 0.001$; $****p \leq 0.0001$).

As folding of aptamers typically depends on the presence of monovalent and bivalent ions, a copper-free, strain-promoted cycloaddition [57] was applied. Aza-DBCO–NHS–ester was used to modify the amino-terminated apt15 and 29 and enabled coupling to azido modified rssp [43] in aqueous buffer (Scheme 1a, Fig. S1a-c). The identity of the apt15-and apt29-rssp conjugates was confirmed using SEC-MALS (Fig. S1d and Table S2). Next, the influence of the chemical coupling on structure and function of the moieties in the apt-rssp conjugates was validated. Because G-rich aptamers typically undergo changes from a random to a G-quadruplex structure depending on ion concentrations, CD spectroscopy was the chosen technique to verify these transformations in the conjugates using ion-depleted (TBE-buffer) and ion-rich conditions (Gq-buffer containing Na^+- and K^+-Ions) [53,54]. Exemplarily, the unmodified as well as the conjugated apt15 revealed clear changes from unstructured to monomeric Q-quadruplex states after transfer into Na^+/K^+-rich buffer, as confirmed by CD spectra with the typical minima at 262 nm and maxima at 290 nm [58,59] (Fig. 1a). The formation of compact G-quadruplex aptamer structures was confirmed by changes in geometric radii (R_g) as evaluated using SEC-MALS analysis in ion-depleted and Na^+/K^+-rich buffers, respectively (Table S2). The proper structures of the aptameric moieties in the soluble conjugates enabled binding of the target protein, as shown by the clear shifts of the

thrombin signal (tryptophan fluorescence, rssp contains no Trp) on the addition of apt15, apt29, or 1:1 mixture of both conjugates (Fig. 1b). Fibrilization of the rssp in the presence of 150 mM potassium phosphate was accompanied by the formation of β-sheet-rich structures [39,43], which was confirmed by CD spectra showing local minimum at 218 nm. Strikingly, the G-quadruplex structure of the aptamer moiety remained intact after fibril formation as indicated by an unchanged maximum at 287 nm (Fig. 1a). The G-quadruplex was accessible on the rssp fibril surface as revealed by TEM. The fibrils incubated with thrombin showed additional associated protein material, whereas no interaction was observed in case of unmodified rssp fibrils (Fig. 1c and d). Self-assembly kinetics (Fig. 1e) indicated slower fibril formation of apt-rssp in comparison to that of the unmodified protein, likely caused by steric hindrance or electrostatic repulsion of the nucleic acids moieties [43]. Strong binding of the aptamers to thrombin consequently affected its enzymatic activity [53–56,60]. Testing the proteolytic cleavage of human fibrinogen and the corresponding formation of insoluble fibrin, apt15-rssp revealed complete inhibition of thrombin due to blockage of the catalytic exosite I. Owing to binding of the apt29 to the regulatory exosite II, the apt29-rssp conjugate only suppressed the thrombin activity in solution (Fig. 1f).

3.2. Aptamer functionalized nanohydrogels for specific target binding

Nanohydrogels made of rssp and apt-rssp were assembled on unmodified and nanofilm-coated substrates (Fig. 2a, setups 1–10). Thrombin (7 nM) was used in combination with HSA (10 μM) in a buffer simulating human serum conditions. The objective was to compare the inhibition efficiency of thrombin binding to the immobilized aptamer ligands and the role of specific as well as unspecific interactions on different substrates. Substrates with and without rssp nanofilms (Fig. 2a [cases 1 and 2]) were incubated in solution of unmodified rssp or aptamer-rssp conjugates in the presence of phosphate ions to trigger self-assembly of the spider silk moiety into nanofibrillar networks (Fig. 1 c a d). The material bound to the substrate after washing (Fig. 2a [cases 3–10]) was tested for thrombin inhibition. Enzymatic activity of free thrombin in solution was sampled using a FRET substrate, i.e. a peptide labeled with fluorescein (5FAM) and a quencher (QXL® 520™) on its C-terminus and N-terminus, respectively (Fig. 1b), allowing fluorescence detection upon the peptide cleavage. Neat (1) and nanofilm-coated substrates (2) as well as unmodified rssp nanofibrils (3 and 4) did not exhibit unspecific thrombin inhibition. However, thrombin activity in solution was significantly diminished on substrates exposing the aptamer-modified fibrils (Fig. 2c–f) self-assembled from apt15-rssp, apt29-rssp, and the respective 1:1 mixture. Whereas nanofibril networks on neat substrates (8–10) revealed 30–51% thrombin activity in comparison to uninhibited enzyme (1–4), only 12–16% of the activity remained in the presence of nanofibrils seeded on rssp nanofilms (5–7). Utilization of the nanofilm support to immobilize nanofibrils resulted in a significant improvement in efficiency and reproducibility of thrombin binding in comparison to that of the nanofibrils on the plain supports (compare cases 5–7 vs. 8–10 in Fig. 2f). Washing the nanofibril networks after their self-assembly randomly removed parts of the fibrillar matrix in samples 8–10 because of their weak unspecific bonding to the polystyrene substrate, highlighting the importance of the seeding approach for anchoring nanohydrogels on substrates. Low residual thrombin activity in samples 5–7 could be ascribed to the K_D of the aptamer ligands and low concentrations of employed thrombin, which were both in a similar nM regime. Thus, further improvement of the target binding is achievable by using ligands with lower K_D (pM), which are potentially obtainable by application of SELEX [13] or engineering of multivalent aptamer nanostructures [61].

AFM measurements of the self-assembled nanofibrils seeded on nanofilms revealed a dense network with a thickness of 45–50 nm. In water, the network formed a nanohydrogel showing significant swelling up to 140–150 nm (Fig. 3a–f, Table S3). The hydrogel-like properties were underlined by changes in the network's deformability as revealed by comparison of the PeakForce Tapping™ measurements in aqueous and dry environments (Fig. S2a-d). Repeated drying/wetting cycles revealed no substantial morphological changes of the nanohydrogels, even heating (40 °C) was employed to accelerate the dehydration between the cycles (Fig. 3g–k). In contrast to the surface-seeded nanohydrogels (<10

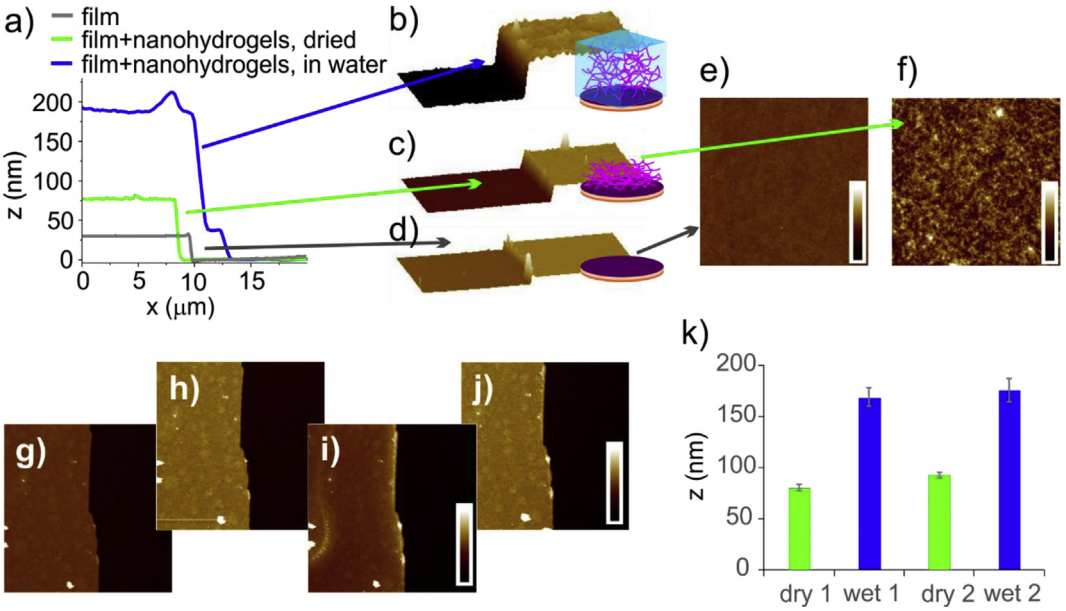

Fig. 3. AFM analysis of nanohydrogels. Spin-coated nanofilms show low roughness (Ra = 0.21 ± 0.02 nm) and thickness (29.7 ± 0.3 nm) (a [grey line], d, and e), respectively. By comparison, the substrate with the nanohydrogel made of apt15-conjugate on top of the rssp nanofilm was 74.3 ± 3.5 nm thick with a roughness of Ra = 2.2 ± 0.17 nm (a [green line], c, and f). Re-immersion into the liquid phase led to increased thickness up to 181 ± 11 nm upon swelling of the nanohydrogel (a [blue line] and b). After the preparation, nanohydrogels were stored at room temperature for 2 months before additional cycles of wetting and drying were applied, revealing reversibility of the nanohydrogel swelling without significant morphological changes (g–k). AFM scans are 5 μm (e and f) and 25 μm (b–d) and 50 μm (g–j) wide. Color bars are in the range from 0 to (e) 10, (f) 25, (g, i) 260, and (h, j) 330 nm.

μM rssp), the formation of bulk hydrogels required much higher concentrations of rssp (typically >200 μM) [32,50,62]. Thus, the formation of immobilized nanohydrogels via surface-triggered nucleation resembles that of surface-assisted assembly of supramolecular hydrogels as described for organic low molecular weight hydrogelators [63].

The inhibitory efficiency of the aptamer-modified nanohydrogels was determined to identify the minimal amount of apt-conjugate required for binding of thrombin. One-component nanohydrogels assembled from single apt15-rssp conjugates were compared to mixed hydrogels co-assembled from unmodified rssp and mixture with apt15-rssp or both apt15-and apt29-rssp conjugates. Clearly, the co-assembly of hydrogels (1–2 μM conjugates) exerted the same thrombin inhibition effect as nanogels based on neat conjugates (10 μM) (Fig. 4a and b). This confirmed that the inhibition on the co-assembled nanohydrogels was not limited by the amount of aptamer ligands, and further improvements to minimize the 'leakage' will be possible by using aptamers with increased affinities. Interestingly, plotting the decreasing thrombin activities on the nanohydrogels against the concentration of the co-assembled apt-rssp conjugates revealed more efficient inhibition in case of mixed aptamers (apt15 and apt29) in comparisons to that of the single aptamer (apt15 hydrogels) (Fig. 4c). Possibly, presence of both aptamers, apt15 and apt29, as well as their spatial vicinity along the fibrils of the rssp networks enabled cooperative binding of the ligands to thrombin exosite I and II. The co-assembly approach enabled controllable incorporation of low levels of the aptamers into rssp hydrogels down to 0.02 μM. This efficacy of the co-assembly will potentially allow incorporation of multiple ligands addressing various low and high affinity targets into rssp fibril networks. The observation of rapid increase of the thrombin activity in solution along with decreased content of the aptamer ligands in the co-assembled nanohydrogels (Fig. 4a and b) implies that the mixed nanohydrogels assembled at 2 μM apt15 yielded almost maximal inhibition capacity revealing 88–90% inactivation of added thrombin (50 ng). In case of nanohydrogels containing both apt15 and apt29, already 1 μM conjugate was sufficient to reach the state of maximal inhibition capacity supporting the cooperative binding hypothesis.

After thrombin deposition, the co-assembled nanohydrogels (labeled I, II III, Fig. 4a) were tested for triggered release of the protease. Therefore, specific oligonucleotides (Table S1) complementary to the thrombin binding aptamer sequence as well as to the T6 linker were designed to open the aptameric structure using strand-replacement [64]. After addition of the complement sequences, an immediate increase of the enzymatic activity was detected in the FRET assays (Fig. 4d and e), revealing low diffusion restrictions for the proteins in the rssp-based nanohydrogels. The triggered release from apt15 functionalized hydrogels (II) using apt15comp probe restored 80% of the thrombin activity in comparison to its initial activity on unmodified nanohydrogels (I). This result revealed the capability of the fibrillar network to prevent thrombin denaturation [65,66] as well as confirmed our previous observation made with GFP-rssp and esterase-rssp fusions that globular proteins remain active upon entrapment in rssp hydrogels [50]. Utilization of the non-complementary oligonucleotide apt29comp, as control probe in case of apt15-modified hydrogel (III), yielded no thrombin release, confirming specificity of the structural change of the aptamer.

4. Conclusion and outlook

Surfaces of spider silk nanofilms made of the rssp eADF4(C16) seeded nanofibril self-assembly and yielded immobilized nanohydrogels. Functionalization with DNA-aptamers enabled specific binding of thrombin under the conditions mimicking blood plasma, whereas the unmodified rssp nanohydrogels revealed no cross-interaction with the target at these conditions. Moreover, addressing the aptamer conformational change using corresponding DNA complements triggered the release of active thrombin from the nanohydrogel depot on demand.

By showing that spider silk coatings are easily accessible on glass, ceramics, metals, alloys, and polymeric materials [49,67–70], the use of rssp nanofilms as coatings represents an attractive approach for fixation

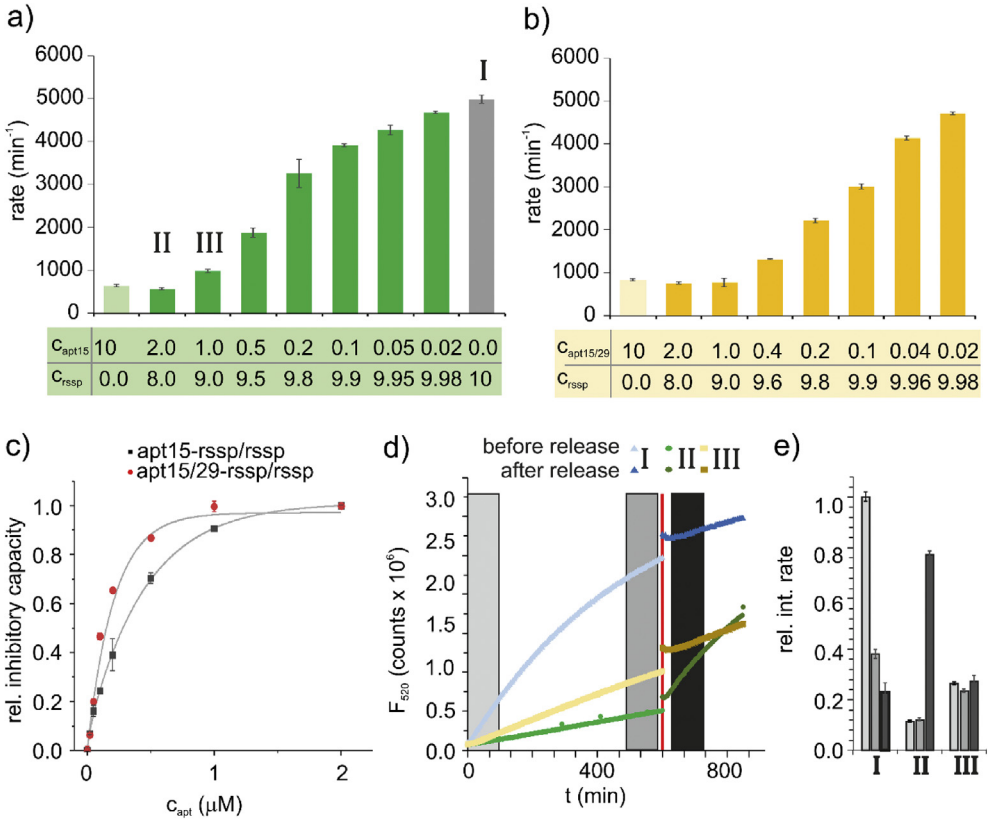

Fig. 4. Cooperative binding and triggered release of thrombin. (a) Thrombin activities on nanohydrogels made of (a) the single apt15-rssp conjugate and (b) 1:1 mixtures of apt15 and apt29-rssp conjugates in combination with unmodified rssp, mixed at concentrations (μM) as indicated below the x axes; (c) relative inhibitory capacities of the nanohydrogels were calculated from thrombin activities in (a and b) and plotted against apt-rssp conjugate; (d and e) the nanohydrogels labeled with mixtures I, II, and III as indicated in (a) were used to test triggered release of thrombin on addition of the matching sequence apt15comp DNA to hydrogels I and II and non-matching sequence apt29comp as III at the timepoint indicated by red line. Relative cleavage rates in (e) were calculated from slopes at different times of the enzymatic reaction as indicated by grey marked areas in (d).

and spatiotemporal control of rssp nanohydrogel formation on any substrate. Moreover, as shown herein as well as in our previous works on oligonucleotide-rssp conjugates [43] or enzyme-rssp fusions [50], self-assembled spider silk fusion hydrogels provide native, i.e. functional structures of coupled biological moieties. As storage and repeating drying/wetting cycles of the nanogels exerted no significant change in their swelling properties and morphology, the presented concept could be suitable for development of nanohydrogel depots for storage and on-demand release of active enzymes [71]. In general, the diversity of potential applications is provided by the diversity of DNA aptamers [13,72,73]. Moreover, aptamers incorporated into hydrogels significantly expand the range of detectable binding events or environmental changes via stimulated structural changes [74] or modified aptamers conjugated with fluorescent dyes, electrochemical indicators, and nanoparticles [51,75]. The underlying rssp also offers additional target anchoring approaches such as genetic modification with enzymes [50], affinity tags [76], or chemical cross-linkers [77]. Thus, the easy-to-immobilize spider silk nanohydrogels in combination with the entire spectrum of accessible aptamers can pave the way for the integration of *per-se* sensitive biocatalysts into biomedical and bioanalytical devices.

Declaration of Competing Interest

The authors declare that they have no known competing financial interests or personal relationships that could have appeared to influence the work reported in this paper.

CRediT authorship contribution statement

M. Humenik: Supervision, Conceptualization, Methodology, Validation, Formal analysis, Investigation, Data curation, Writing - Original draft, Writing - Review and Editing, Visualization, Funding acquisition. **T. Preiß:** Investigation, Validation, Data curation. **S. Gödrich:** Investigation, Validation, Data curation, Writing - Review and Editing. **G. Papastavrou:** Writing – Review & Editing, Resources. **T. Scheibel:** Writing – Review & Editing, Resources, Funding acquisition.

Acknowledgments

This work was financially supported by the DFG grant SFB 840 TP A8 as well as the EU grand EFRE, Ziel ETZ 2014–2020, Freistaat Bayern—Tschechien, Project Nr. 123. The authors thank Dr. Tamara Aigner for TEM and Demetrio Piro for assistance with the coagulation assay and the assembly of the nanohydrogels on Si-wafers.

Appendix A. Supplementary data

Supplementary data to this article can be found online at https://doi.org/10.1016/j.mtbio.2020.100045.

References

[1] S.J. Updike, G.P. Hicks, The enzyme electrode, Nature 214 (5092) (1967) 986–988.
[2] E. Engvall, P. Perlmann, Enzyme-linked immunosorbent assay (ELISA) quantitative assay of immunoglobulin G, Immunochemistry 8 (9) (1971) 871–874.
[3] T. Sano, C.L. Smith, C.R. Cantor, Immuno-PCR: very sensitive antigen detection by means of specific antibody-DNA conjugates, Science 258 (5079) (1992) 120.
[4] C.M. Niemeyer, M. Adler, R. Wacker, Immuno-PCR: high sensitivity detection of proteins by nucleic acid amplification, Trends Biotechnol. 23 (4) (2005) 208–216.
[5] C. Pohlmann, Y. Wang, M. Humenik, B. Heidenreich, M. Gareis, M. Sprinzl, Rapid, specific and sensitive electrochemical detection of foodborne bacteria, Biosens. Bioelectron. 24 (9) (2009) 2766–2771.
[6] J.P. Chambers, B.P. Arulanandam, L.L. Matta, A. Weis, J.J. Valdes, Biosensor recognition elements, Curr. Issues Mol. Biol. 10 (1–2) (2008) 1–12.
[7] M.A. Morales, J.M. Halpern, Guide to selecting a biorecognition element for biosensors, Bioconjugate Chem. 29 (10) (2018) 3231–3239.
[8] A. De Girolamo, M. McKeague, M. Pascale, M. Cortese, M.C. DeRosa, Immobilization of Aptamers on Substrates, Aptamers for Analytical Applications: Affinity Acquisition and Method Design, 2018, pp. 85–126.
[9] V. Crivianu-Gaita, M. Thompson, Aptamers, antibody scFv, and antibody Fab' fragments: an overview and comparison of three of the most versatile biosensor biorecognition elements, Biosens. Bioelectron. 85 (2016) 32–45.
[10] Y. Wu, I. Belmonte, K.S. Sykes, Y. Xiao, R.J. White, Perspective on the future role of aptamers in analytical chemistry, Anal. Chem. 91 (24) (2019) 15335–15344.
[11] P.S. Sharma, Z. Iskierko, A. Pietrzyk-Le, F. D'Souza, W. Kutner, Bioinspired intelligent molecularly imprinted polymers for chemosensing: a mini review, Electrochem. Commun. 50 (2015) 81–87.
[12] A.D. Ellington, J.W. Szostak, In vitro selection of RNA molecules that bind specific ligands, Nature 346 (6287) (1990) 818–822.
[13] L.C. Bock, L.C. Griffin, J.A. Latham, E.H. Vermaas, J.J. Toole, Selection of single-stranded DNA molecules that bind and inhibit human thrombin, Nature 355 (6360) (1992) 564–566.
[14] S.M. Shamah, J.M. Healy, S.T. Cload, Complex target SELEX, Acc. Chem. Res. 41 (1) (2008) 130–138.
[15] R. Stoltenburg, C. Reinemann, B. Strehlitz, SELEX-A (r)evolutionary method to generate high-affinity nucleic acid ligands, Biomol. Eng. 24 (4) (2007) 381–403.
[16] A.M. Horgan, J.D. Moore, J.E. Noble, G.J. Worsley, Polymer- and colloid-mediated bioassays, sensors and diagnostics, Trends Biotechnol. 28 (9) (2010) 485–494.
[17] C.A. DeForest, D.A. Tirrell, A photoreversible protein-patterning approach for guiding stem cell fate in three-dimensional gels, Nat. Mater. 14 (2015) 523.
[18] A. Shastri, L.M. McGregor, Y. Liu, V. Harris, H. Nan, M. Mujica, Y. Vasquez, A. Bhattacharya, Y. Ma, M. Aizenberg, O. Kuksenok, A.C. Balazs, J. Aizenberg, X. He, An aptamer-functionalized chemomechanically modulated biomolecule catch-and-release system, Nat. Chem. 7 (2015) 447.
[19] C.D. Blanchette, J.M. Knipe, J.K. Stolaroff, J.R. DeOtte, J.S. Oakdale, A. Maiti, J.M. Lenhardt, S. Sirajuddin, A.C. Rosenzweig, S.E. Baker, Printable enzyme-embedded materials for methane to methanol conversion, Nat. Commun. 7 (2016) 11900.
[20] Y.S. Zhang, A. Khademhosseini, Advances in engineering hydrogels, Science 356 (6337) (2017) eaaf3627.
[21] I.Y. Jung, J.S. Kim, B.R. Choi, K. Lee, H. Lee, Hydrogel based biosensors for in vitro diagnostics of biochemicals, proteins, and genes, Adv. Healthcare Mater. 6 (12) (2017) 1601475.
[22] R.V. Ulijn, N. Bibi, V. Jayawarna, P.D. Thornton, S.J. Todd, R.J. Mart, A.M. Smith, J.E. Gough, Bioresponsive hydrogels, Mater. Today 10 (4) (2007) 40–48.
[23] L.A. Estroff, A.D. Hamilton, Water gelation by small organic molecules, Chem. Rev. 104 (3) (2004) 1201–1218.
[24] E. Prince, E. Kumacheva, Design and applications of man-made biomimetic fibrillar hydrogels, Nat. Rev. Mater. 4 (2) (2019) 99–115.
[25] H. Cui, M.J. Webber, S.I. Stupp, Self-assembly of peptide amphiphiles: from molecules to nanostructures to biomaterials, Pept. Sci. 94 (1) (2010) 1–18.
[26] G.C. Le Goff, R.L. Srinivas, W.A. Hill, P.S. Doyle, Hydrogel microparticles for biosensing, Eur. Polym. J. 72 (2015) 386–412.
[27] G. Sudre, L. Olanier, Y. Tran, D. Hourdet, C. Creton, Reversible adhesion between a hydrogel and a polymer brush, Soft Matter 8 (31) (2012) 8184–8193.
[28] H. Yuk, T. Zhang, G.A. Parada, X. Liu, X. Zhao, Skin-inspired hydrogel–elastomer hybrids with robust interfaces and functional microstructures, Nat. Commun. 7 (2016) 12028.
[29] W. Huang, A. Tarakanova, N. Dinjaski, Q. Wang, X. Xia, Y. Chen, J.Y. Wong, M.J. Buehler, D.L. Kaplan, Design of multistimuli responsive hydrogels using integrated modeling and genetically engineered silk–elastin-like proteins, Adv. Funct. Mater. 26 (23) (2016) 4113–4123.
[30] L.E.R. O'Leary, J.A. Fallas, E.L. Bakota, M.K. Kang, J.D. Hartgerink, Multi-hierarchical self-assembly of a collagen mimetic peptide from triple helix to nanofibre and hydrogel, Nat. Chem. 3 (2011) 821.
[31] J.D. Hartgerink, E. Beniash, S.I. Stupp, Self-assembly and mineralization of peptide-amphiphile nanofibers, Science 294 (5547) (2001) 1684.
[32] K. Schacht, T. Scheibel, Controlled hydrogel formation of a recombinant spider silk protein, Biomacromolecules 12 (7) (2011) 2488–2495.
[33] B. Yang, D.J. Adams, M. Marlow, M. Zelzer, Surface-Mediated supramolecular self-assembly of protein, peptide, and nucleoside derivatives: from surface design to the underlying mechanism and tailored functions, Langmuir 34 (50) (2018) 15109–15125.
[34] A. Keller, M. Fritzsche, Y.-P. Yu, Q. Liu, Y.-M. Li, M. Dong, F. Besenbacher, Influence of hydrophobicity on the surface-catalyzed assembly of the islet amyloid polypeptide, ACS Nano 5 (4) (2011) 2770–2778.
[35] L. Shen, T. Adachi, D. Vanden Bout, X.Y. Zhu, A mobile precursor determines amyloid-β peptide fibril formation at interfaces, J. Am. Chem. Soc. 134 (34) (2012) 14172–14178.
[36] R. Hajiraissi, M. Hanke, A. Gonzalez Orive, B. Duderija, U. Hofmann, Y. Zhang, G. Grundmeier, A. Keller, Effect of terminal modifications on the adsorption and assembly of hIAPP(20–29), ACS Omega 4 (2) (2019) 2649–2660.
[37] Y.-C. Lin, E.J. Petersson, Z. Fakhraai, Surface effects mediate self-assembly of amyloid-β peptides, ACS Nano 8 (10) (2014) 10178–10186.
[38] T.T.H. Pham, W.H. Rombouts, R. Fokkink, M.C.A. Stuart, M.A. Cohen Stuart, J.M. Kleijn, Nanoparticle-templated formation and growth mechanism of curved protein polymer fibrils, Biomacromolecules 17 (7) (2016) 2392–2398.
[39] M. Humenik, A.M. Smith, S. Arndt, T. Scheibel, Ion and seed dependent fibril assembly of a spidroin core domain, J. Struct. Biol. 4 (2015) 571–576.
[40] A. Molina, T. Scheibel, M. Humenik, Nanoscale patterning of surfaces via DNA directed spider silk assembly, Biomacromolecules 20 (1) (2019) 347–352.
[41] A. Pica, I. Russo Krauss, V. Parente, H. Tateishi-Karimata, S. Nagatoishi, K. Tsumoto, N. Sugimoto, F. Sica, Through-bond effects in the ternary complexes of thrombin sandwiched by two DNA aptamers, Nucleic Acids Res. 45 (1) (2017) 461–469.

[42] U.K. Slotta, S. Rammensee, S. Gorb, T. Scheibel, An engineered spider silk protein forms microspheres, Angew. Chem. Int. Ed. 47 (24) (2008) 4592–4594.
[43] M. Humenik, T. Scheibel, Nanomaterial building blocks based on spider silk–oligonucleotide conjugates, ACS Nano 8 (2) (2014) 1342–1349.
[44] M. Humenik, M. Drechsler, T. Scheibel, Controlled hierarchical assembly of spider silk-DNA chimeras into ribbons and raft-like morphologies, Nano Lett. 14 (7) (2014) 3999–4004.
[45] M. Humenik, M. Magdeburg, T. Scheibel, Influence of repeat numbers on self-assembly rates of repetitive recombinant spider silk proteins, J. Struct. Biol. 186 (2014) 431–437.
[46] A. Roloff, A.S. Carlini, C.E. Callmann, N.C. Gianneschi, Micellar thrombin-binding aptamers: reversible nanoscale Anticoagulants, J. Am. Chem. Soc. 139 (46) (2017) 16442–16445.
[47] Y.-C. Shiang, C.-C. Huang, T.-H. Wang, C.-W. Chien, H.-T. Chang, Aptamer-conjugated nanoparticles efficiently control the activity of thrombin, Adv. Funct. Mater. 20 (18) (2010) 3175–3182.
[48] K. Spiess, R. Ene, C.D. Keenan, J. Senker, F. Kremer, T. Scheibel, Impact of initial solvent on thermal stability and mechanical properties of recombinant spider silk films, J. Mater. Chem. 21 (35) (2011) 13594–13604.
[49] C.B. Borkner, S. Lentz, M. Müller, A. Fery, T. Scheibel, Ultra-thin spider silk films: insights into spider silk assembly on surfaces, ACS Appl. Polym. Mater. 1 (12) (2019) 3366–3374.
[50] M. Humenik, M. Mohrand, T. Scheibel, Self-assembly of spider silk-fusion proteins comprising enzymatic and fluorescence activity, Bioconjugate Chem. 29 (4) (2018) 898–904.
[51] F. Wang, X. Liu, I. Willner, DNA switches: from principles to applications, Angew. Chem. Int. Ed. 54 (4) (2015) 1098–1129.
[52] S. Li, Q. Jiang, S. Liu, Y. Zhang, Y. Tian, C. Song, J. Wang, Y. Zou, G.J. Anderson, J.-Y. Han, Y. Chang, Y. Liu, C. Zhang, L. Chen, G. Zhou, G. Nie, H. Yan, B. Ding, Y. Zhao, A DNA nanorobot functions as a cancer therapeutic in response to a molecular trigger in vivo, Nat. Biotechnol. 36 (2018) 258–264.
[53] D.M. Tasset, M.F. Kubik, W. Steiner, Oligonucleotide inhibitors of human thrombin that bind distinct epitopes, J. Mol. Biol. 272 (5) (1997) 688–698.
[54] R.F. Macaya, P. Schultze, F.W. Smith, J.A. Roe, J. Feigon, Thrombin-binding DNA aptamer forms a unimolecular quadruplex structure in solution, Proc. Natl. Acad. Sci. U. S. A. 90 (8) (1993) 3745.
[55] Y.-C. Shiang, C.-L. Hsu, C.-C. Huang, H.-T. Chang, Gold nanoparticles presenting hybridized self-assembled aptamers that exhibit enhanced inhibition of thrombin, Angew. Chem. Int. Ed. 50 (33) (2011) 7660–7665.
[56] A. Trapaidze, J.-P. Hérault, J.-M. Herbert, A. Bancaud, A.-M. Gué, Investigation of the selectivity of thrombin-binding aptamers for thrombin titration in murine plasma, Biosens. Bioelectron. 78 (2016) 58–66.
[57] E.M. Sletten, C.R. Bertozzi, Bioorthogonal chemistry: fishing for selectivity in a sea of functionality, Angew. Chem. Int. Ed. 48 (38) (2009) 6974–6998.
[58] J. Kypr, I. Kejnovská, D. Renčiuk, M. Vorlíčková, Circular dichroism and conformational polymorphism of DNA, Nucleic Acids Res. 37 (6) (2009) 1713–1725.
[59] V. Dapić, V. Abdomerović, R. Marrington, J. Peberdy, A. Rodger, J.O. Trent, P.J. Bates, Biophysical and biological properties of quadruplex oligodeoxyribonucleotides, Nucleic Acids Res. 31 (8) (2003) 2097–2107.
[60] V. Parente, A. Pica, I. Russo Krauss, F. Sica, H. Tateishi-Karimata, S. Nagatoishi, N. Sugimoto, K. Tsumoto, Through-bond effects in the ternary complexes of thrombin sandwiched by two DNA aptamers, Nucleic Acids Res. 45 (1) (2016) 461–469.
[61] A. Rangnekar, A.M. Zhang, S.S. Li, K.M. Bompiani, M.N. Hansen, K.V. Gothelf, B.A. Sullenger, T.H. LaBean, Increased anticoagulant activity of thrombin-binding DNA aptamers by nanoscale organization on DNA nanostructures, Nanomed. Nanotechnol. Biol. Med. 8 (5) (2012) 673–681.
[62] K. Schacht, T. Jüngst, M. Schweinlin, A. Ewald, J. Groll, T. Scheibel, Biofabrication of cell-loaded 3D spider silk constructs, Angew. Chem. Int. Ed. 54 (9) (2015) 2816–2820.
[63] C. Vigier-Carrière, F. Boulmedais, P. Schaaf, L. Jierry, Surface-assisted self-assembly strategies leading to supramolecular hydrogels, Angew. Chem. Int. Ed. 57 (6) (2018) 1448–1456.
[64] D.Y. Zhang, E. Winfree, Control of DNA strand displacement kinetics using toehold exchange, J. Am. Chem. Soc. 131 (47) (2009) 17303–17314.
[65] Y. Liu, J. Yu, Oriented immobilization of proteins on solid supports for use in biosensors and biochips: a review, Microchim. Acta 183 (1) (2016) 1–19.
[66] N.R. Mohamad, N.H.C. Marzuki, N.A. Buang, F. Huyop, R.A. Wahab, An overview of technologies for immobilization of enzymes and surface analysis techniques for immobilized enzymes, Biotechnol. Biotechnol. Equip. 29 (2) (2015) 205–220.
[67] S. Wohlrab, Spie, T. Scheibel, Varying surface hydrophobicities of coatings made of recombinant spider silk proteins, J. Mater. Chem. 22 (41) (2012) 22050–22054.
[68] C.B. Borkner, M.B. Elsner, T. Scheibel, Coatings and films made of silk proteins, ACS Appl. Mater. Interfaces 6 (18) (2014) 15611–15625.
[69] C.B. Borkner, S. Wohlrab, E. Möller, G. Lang, T. Scheibel, Surface modification of polymeric biomaterials using recombinant spider silk proteins, ACS Biomater. Sci. Eng. 3 (5) (2017) 767–775.
[70] R.H. Zha, P. Delparastan, T.D. Fink, J. Bauer, T. Scheibel, P.B. Messersmith, Universal nanothin silk coatings via controlled spidroin self-assembly, Biomater. Sci. 7 (2) (2019) 683–695.
[71] W. Bai, N.A. Gariano, D.A. Spivak, Macromolecular amplification of binding response in superaptamer hydrogels, J. Am. Chem. Soc. 135 (18) (2013) 6977–6984.
[72] A.D. Keefe, S. Pai, A. Ellington, Aptamers as therapeutics, Nat. Rev. Drug Discov. 9 (2010) 537.
[73] D.H.J. Bunka, P.G. Stockley, Aptamers come of age - at last, Nat. Rev. Microbiol. 4 (8) (2006) 588–596.
[74] J. Li, L. Mo, C.-H. Lu, T. Fu, H.-H. Yang, W. Tan, Functional nucleic acid-based hydrogels for bioanalytical and biomedical applications, Chem. Soc. Rev. 45 (5) (2016) 1410–1431.
[75] A.-K. Schneider, C.M. Niemeyer, DNA surface technology – from gene sensors to integrated systems for life science and materials research, Angew. Chem. Int. Ed. 57 (52) (2018) 16959–16967.
[76] M. Lucke, I. Mottas, T. Herbst, C. Hotz, L. Römer, M. Schierling, H.M. Herold, U. Slotta, T. Spinetti, T. Scheibel, G. Winter, C. Bourquin, J. Engert, Engineered hybrid spider silk particles as delivery system for peptide vaccines, Biomaterials 172 (2018) 105–115.
[77] K. Spiess, S. Wohlrab, T. Scheibel, Structural characterization and functionalization of engineered spider silk films, Soft Matter 6 (17) (2010) 4168–4174.